3D Prostate Segmentation of Ultrasound Images Combining Longitudinal Image Registration and Machine Learning

Xiaofeng Yang [1] and Baowei Fei [1,2,*]

[1]Department of Radiology and Imaging Sciences, Emory University, Atlanta, GA
[2]Department of Biomedical Engineering, Emory University and Georgia Institute of Technology,
* Corresponding author: email: bfei@emory.edu, website: http://feilab.org

ABSTRACT

We developed a three-dimensional (3D) segmentation method for transrectal ultrasound (TRUS) images, which is based on longitudinal image registration and machine learning. Using longitudinal images of each individual patient, we register previously acquired images to the new images of the same subject. Three orthogonal Gabor filter banks were used to extract texture features from each registered image. Patient-specific Gabor features from the registered images are used to train kernel support vector machines (KSVMs) and then to segment the newly acquired prostate image. The segmentation method was tested in TRUS data from five patients. The average surface distance between our and manual segmentation is 1.18 ± 0.31 mm, indicating that our automatic segmentation method based on longitudinal image registration is feasible for segmenting the prostate in TRUS images.

Keywords: Transrectal ultrasound (TRUS), image registration, prostate cancer, machine learning, image segmentation, support vector machine (SVM)

1. INTRODUCTION

Prostate cancer is the second leading cause of cancer death in men in the United States [1]. Transrectal ultrasound (TRUS)-guided biopsy is the clinical standard for definitive diagnosis of prostate cancer. While two-dimensional (2D) TRUS-guided biopsy is routinely performed, however, 2D ultrasound images do not provide three-dimensional (3D) location information of the biopsy sample. Consequently, the physician must mentally estimate the 3D location of the biopsy needle based on limited 2D information, thus leading to suboptimal biopsy targeting. Three-dimensional transrectal ultrasound images have been used to guide prostate biopsy [2, 3] or therapy [4, 5]. Another challenge for TRUS-guided biopsy is that ultrasound imaging cannot reliably detect prostate cancer and thus cannot be used to guide targeted biopsy. Other imaging modalities such as positron emission tomography (PET) has been used to detect prostate cancer. Various PET imaging agents have been developed for prostate cancer detection and staging, these include anti-1-amino-3-^{18}F-fluorocyclobutane-1-carboxylic acid (^{18}F-FACBC) [6, 7], ^{11}C-choline [8, 9], ^{18}F-fluorocholine [10], ^{11}C-acetate [11], ^{11}C-methionine [12], and other PET agents. By combining PET/CT with 3D ultrasound images, multimodality image-guided targeted biopsy may be able to improve the detection of prostate cancer as recently reported by us [3].

In order to build a 3D model from ultrasound images for TRUS-guided biopsy, segmentation of the prostate is required. Segmentation of the prostate in ultrasound images can be difficult because of the shadows from the bladder and because of a low contrast between the prostate and non-prostate tissue. Many methods were proposed to automatically segment the prostate in ultrasound images [13-31]. A semiautomatic method by warping an ellipse to fit the prostate on TRUS images was previously presented by Badiei et al [32]. A 2D semiautomatic discrete dynamic contour model was used to segment the prostate [33]. Level-set based methods [27, 34] also were used to detect the prostate surface from 3D ultrasound images. Gabor support vector machine (G-SVM) and statistical shape model were used to extract the prostate boundary [35, 36]. Accurate segmentation of the prostate plays a key role in biopsy needle placement and treatment planning [26, 37]. In this study, we developed a 3D segmentation method for prostate ultrasound images, which is based on longitudinal image registration and machine learning.

Medical Imaging 2012: Image-Guided Procedures, Robotic Interventions, and Modeling,
edited by David R. Holmes III, Kenneth H. Wong, Proc. of SPIE Vol. 8316, 83162O

2. METHODS

Our segmentation method consists of three major components: (1) Longitudinal image registration, (2) Hierarchical representation of image features using Gabor filter banks, and (3) Training of kernel support vector machine (KSVM). Figure 1 shows a schematic flow chart of our method. The steps are briefly described as follows.

(1) Register the previously acquired TRUS image, e.g. pre-biopsy image, to the newly acquired TRUS image, e.g. intra-biopsy image. In our group, a variety of rigid and nonrigid registration methods have been validated for prostate image registration [38-45]. In this study, we developed a deformable registration method [46] for this particular application, which is used to obtain the spatial deformation field between the intra-biopsy image and pre-biopsy image. The same transformation is applied to the segmented prostate surface in the pre-biopsy data. Use a histogram matching algorithm, the intensity of pre-biopsy TRUS image is matched to the intensity of the intra-biopsy TRUS image.

(2) Apply three Gabor filters in three orthogonal planes to extract prostate features from the registered image as well as from the newly acquired TRUS image. Every TRUS image is divided into *n* 3D sub-regions overlapped with each other. Every 3D sub-region has three sub-volumes of Gabor features in the three orthogonal planes.

(3) Train and apply the kernel support vector machines (KSVM) for segmentation. Once the KSVMs are trained with the three sub-volumes of each sub-region in the pre-biopsy images, they are applied to the corresponding sub-volumes of the same sub-region in the newly acquired TRUS image in order to segment the prostate.

Gabor filter banks are used to capture image features in multiple scales and multiple orientations [47]. To save computation time and also reasonably approximate the complete set of 3D Gabor features, we use three banks of 2D Gabor filters located in the three orthogonal planes (Figure 2). The three selected filter banks are orthogonal or parallel to the axis of the ultrasound probe. Below, 2D Gabor filter banks in the transverse plane are described as follows [30]:

$$t(x,y)=\frac{1}{2\pi\sigma_x\sigma_y}\exp[-\frac{1}{2}(\frac{x^2}{\sigma_x^2}+\frac{y^2}{\sigma_y^2})+2\pi\sqrt{-1}(u_0x+v_0y)] \quad (1)$$

Where (u_0, v_0) is the spatial frequency of the filter in the frequency domain, and σ_x and σ_y are the standard deviation of the Gaussian function. Similarly, the 2D Gabor filter banks in the other two orthogonal planes can be described as $g(y,z)$ and $h(x,z)$, respectively. When applying the above Gabor filter banks to an individual voxel τ, three sets of texture features are obtained, which correspond to the real and imaginary parts of the three orthogonal filter banks:

$$\{T_{\lambda,\theta}^{real}(\tau)\},\ \{T_{\lambda,\theta}^{imag}(\tau)\},\ \{G_{\lambda,\theta}^{real}(\tau)\},\ \{G_{\lambda,\theta}^{imag}(\tau)\},\ \{H_{\lambda,\theta}^{real}(\tau)\},\ \{H_{\lambda,\theta}^{imag}(\tau)\} \quad (2)$$

Where λ and θ are the number of the scales and orientations, respectively. Figure 3 shows the extracted Gabor features from an example TRUS image. Notably, although certain Gabor filters can be modeled as orientation and scale tunable edge detectors or smoothing filters, the micro-features extracted by these filters in a given region often jointly characterize the underlying texture information.

Kernal support vector machine (KSVM) is a statistical classification method proposed by Vapnik [48]. Given *m* samples, KSVM can create a nonlinear decision plane that optimally separates the positive samples from negative samples based on the statistical learning theory. We use a number of KSVMs, each of which is applied to a 3D sub-region in the TRUS image. Particularly, the entire TRUS image is uniformly divided into sub-regions that are designed to be overlapped with each other. Each KSVM is trained by Gabor texture feature vectors extracted from prostate tissue and non-prostate tissue, respectively. During the training stage, the texture priors of the prostate and non-prostate samples are implicitly characterized. The pre-trained KSVM is then used to label tissue at each voxel according to its corresponding Gabor texture feature vector. The KSVM outputs a real value that is nonlinearly mapped to [0, 1], indicating the likelihood of the voxel belonging to the prostate tissue.

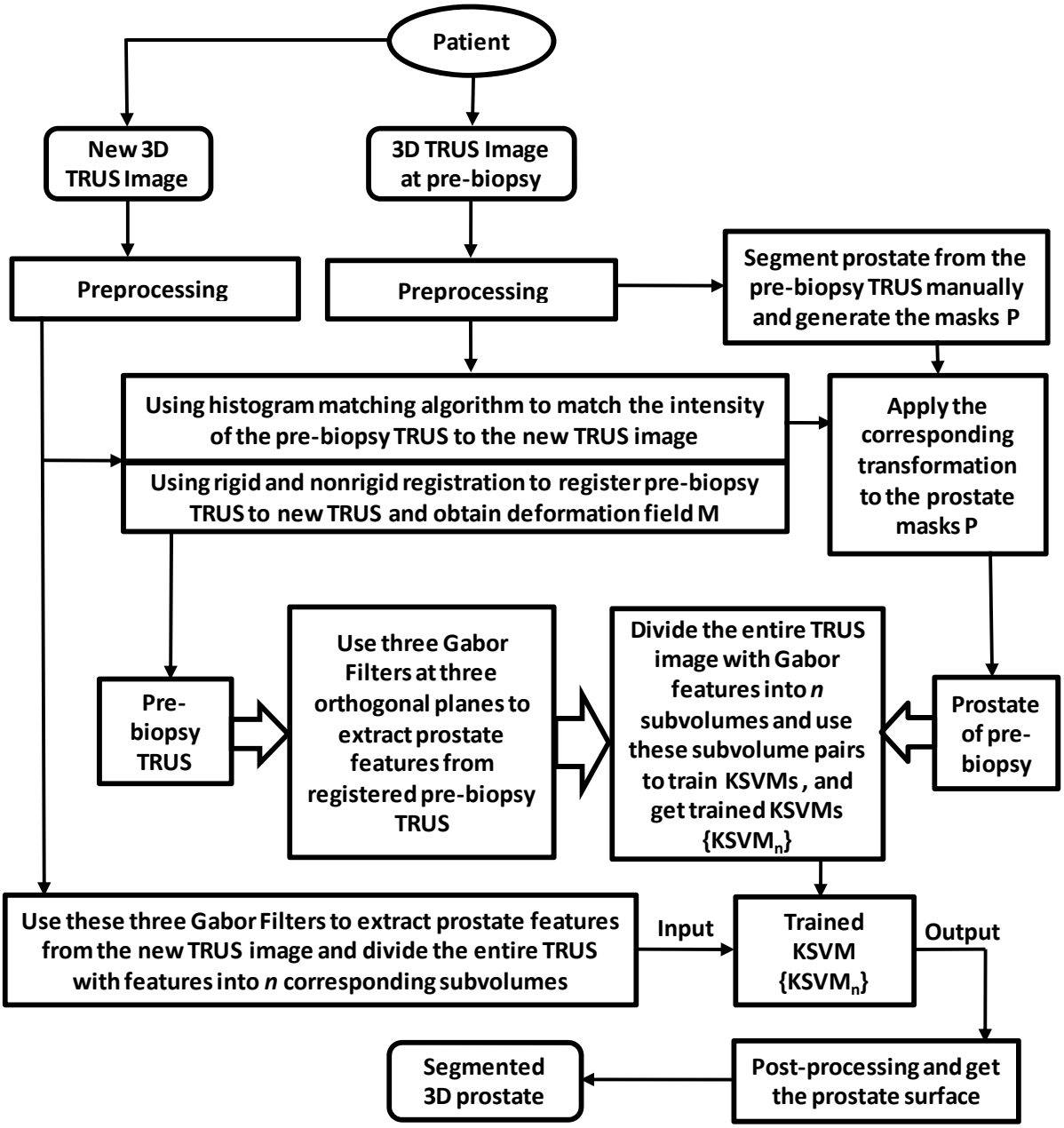

Figure 1. Schematic flow chart of the proposed algorithm for 3D segmentation of the prostate.

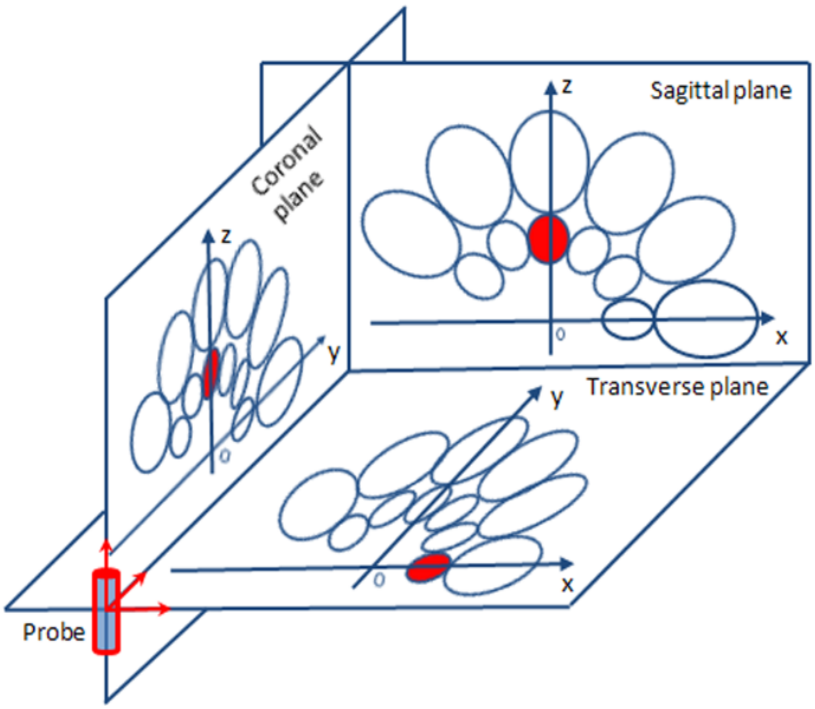

Figure 2. The frequency spectra of three orthogonal banks of 2D Gabor filters located in three orthogonal planes. The ellipse contour denotes the half-peak magnitude of the filter responses. The axes x, y, and z denote the three orthogonal directions, respectively.

3. RESULTS

We apply the segmentation method to five patients' TRUS images (matrix: $224\times224\times175$, $0.380\times0.380\times0.390$ mm^3/voxel) that were acquired pre- and post-biopsy. In our implementation, 36 KSVMs are attached to 36 sub-regions. The number of orientation and scales are 6 and 3 for the Gabor filter, respectively. In our experiment, we used pre-biopsy images to segment post-biopsy images. Five corresponding post-biopsy images were used for evaluation. The automatic segmentation results were evaluated by the manual segmentation results. Dice overlap ratio was used as the metric to evaluate the performance of the segmentation [49-51].

Figure 4 shows the nonrigid registration result between the newly acquired TRUS image (post-biopsy) and previously acquired image (pre-biopsy). As the 3D images at different time points have different sizes of the prostate and their TRUS images may be acquired at slightly different position and orientation, the nonrigid registration (translations, rotations, scaling, and deformation) is able to normalize the image. Figure 5 shows the segmentation results for one patient. The results from the automatic segmentation methods are close to the manual segmentation.

Table 1 provides the quantitative evaluation results of the segmentation method for the five patients. The average surface distances range from 0.88 mm to 1.63 mm with a mean distance of 1.18 mm. The root mean squares (RMS) vary from 1.14 mm to 1.93 mm with a mean of 1.43 mm. The maximum distance (MAX) is less than 5.00 mm for the five patients. The Dice ratios range from 87.0% to 90.2% with a mean of 88.1%.

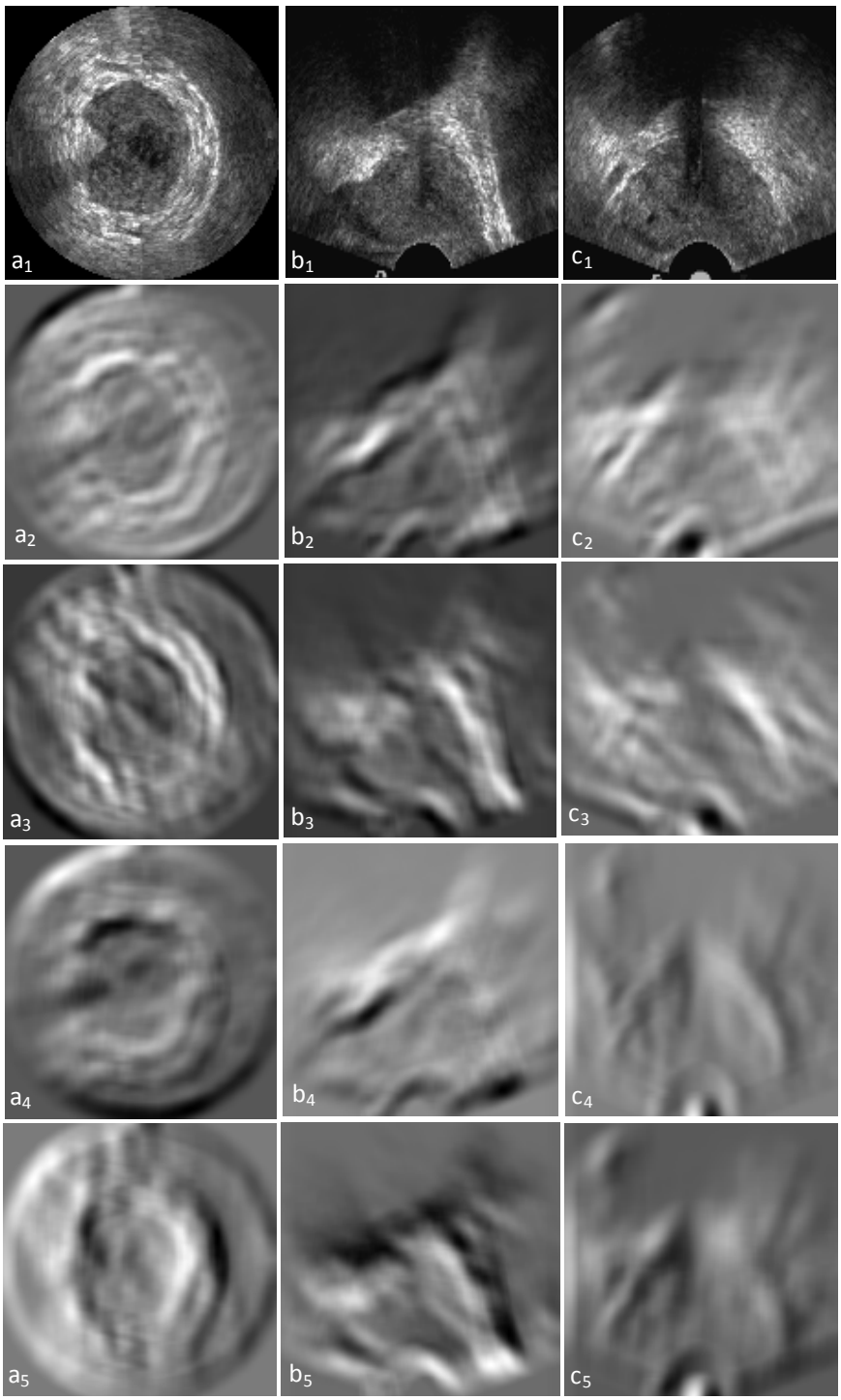

Figure 3. Gabor features extracted by three orthogonal Gabor filter banks. *Left:* From top (a_1) to bottom (a_5), the transverse image, the Gabor features of the two real components ($H_{4,1}^{real}$ and $H_{4,4}^{real}$) and the two imaginary ($H_{5,2}^{imag}$ and $H_{5,3}^{imag}$) components, respectively. *Middle and right*: The TRUS images and the Gabor features in the coronal and saggital orientations, respectively.

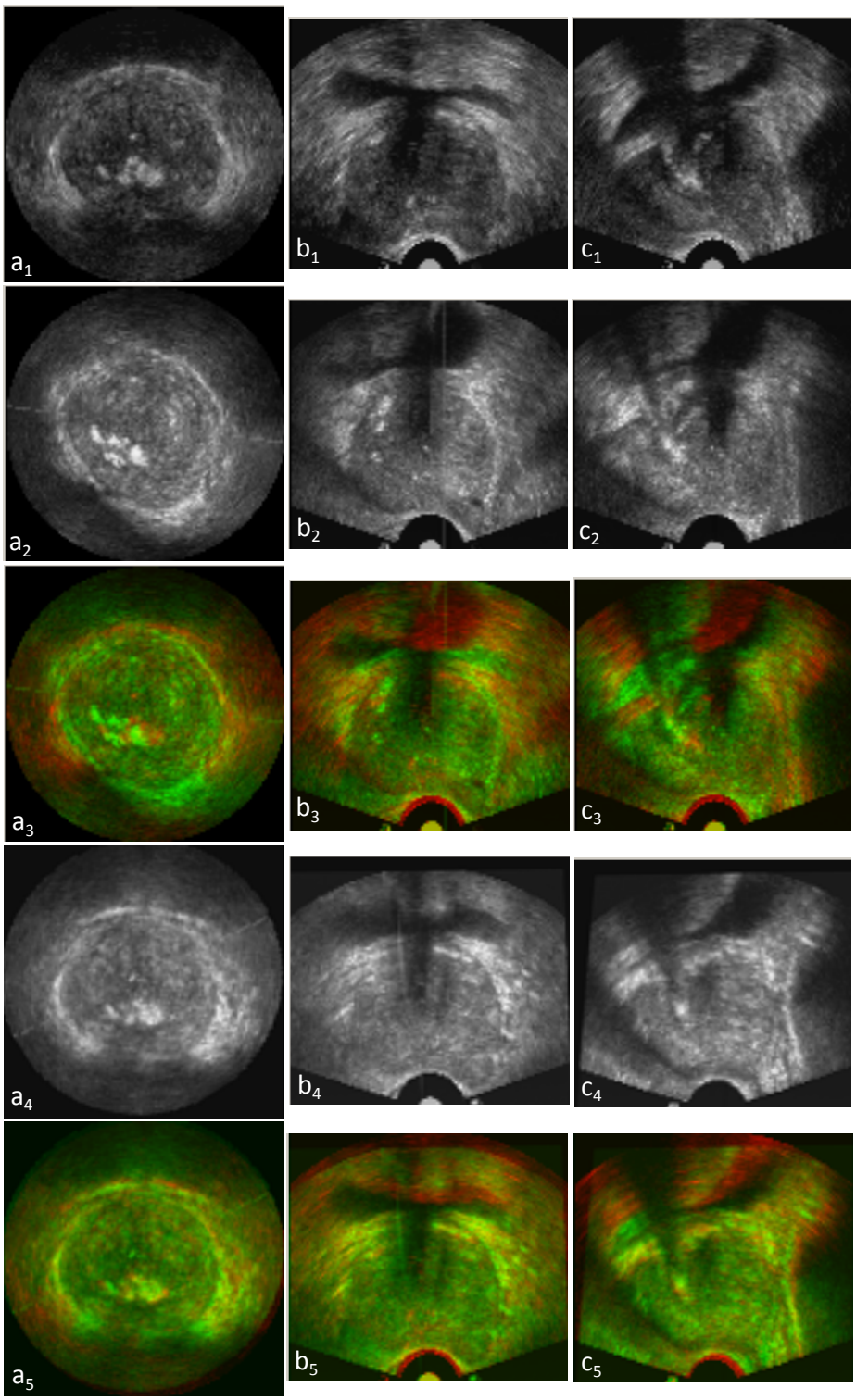

Figure 4. Visual assessment of 3D TRUS registration. a_1, b_1 and c_1 are post-biopsy images in three directions. a_2, b_2 and c_2 are pre-biopsy images, and a_3, b_3 and c_3 are the fusion images between pre- and post-biopsy images. a_4, b_4 and c_4 are the 3D registered pre-biopsy images; and a_5, b_5 and c_5 are the fusion images between registered pre- and post-biopsy images.

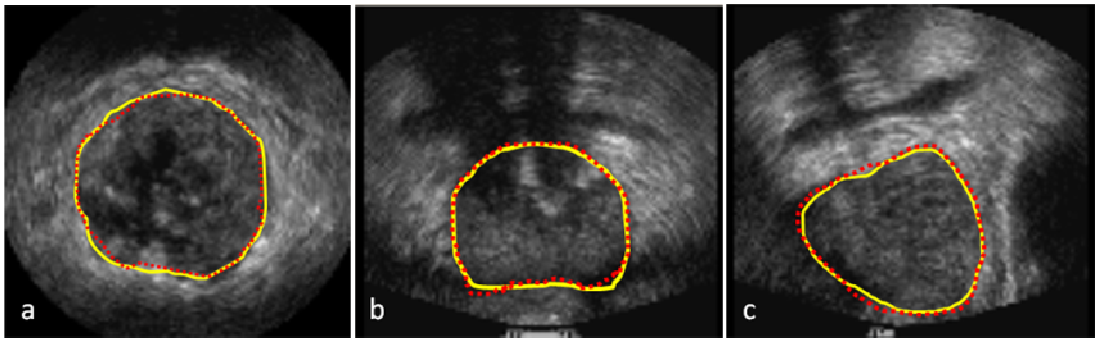

Figure 5. Comparison between the proposed method and manual segmentation. Images from left to right are in three orientations of the same TRUS image volume. The line in yellow is the manual segmentation result. The dashed line in red is the segmentation result of the proposed method.

Table 1. Comparison between our and manual segmentations.

Patients ID	Surface Distance (mm)			Dice (%)
	Average	RMS	Max	
28	1.63	1.93	4.72	87.0
23	1.37	1.54	3.03	87.3
32	0.97	1.30	4.39	89.1
17	0.88	1.14	3.42	90.2
25	1.03	1.28	3.92	87.1
Mean ± STD	1.18±0.31	1.43±0.31	3.89±0.70	88.1±1.44

4. CONCLUSIN

This paper presented an automatic, 3D segmentation method for prostate TRUS images based on longitudinal image registration. Using longitudinal images for each individual subject, we registered previously acquired images to newly acquired images of the same subject. Patient-specific Gabor features from the images at different time points were used to train kernel support vector machines (KSVMs) and then to segment the newly acquired prostate image. Validation on patient data shows that our approach is able to accurately and robustly segment the prostate from TRUS images. As the patient-specific pre-biopsy TRUS image is used to train the kernel support vector machines for automatic segmentation, the robustness and accuracy of the algorithm is improved. The reliability of the segmentation method does not depend on any initialization step. We are integrating the proposed segmentation method into our 3D ultrasound-guided biopsy system.

ACKNOWLEGEMENT

This research is supported in part by NIH grant R01CA156775 (PI: Fei), Georgia Cancer Coalition Distinguished Clinicians and Scientists Award (PI: Fei), The Emory Molecular and Translational Imaging Center (NIH P50CA128301). We thank Dr. Aaron Fenster at the Robarts Research Institute of The University of Western Ontario for providing the ultrasound images.

REFERENCES

[1] Jemal, A., R. Siegel, J. Xu *et al.*, "Cancer statistics, 2010," CA Cancer J.Clin., 60(5), 277-300 (2010).

[2] Cool, D., S. Sherebrin, J. Izawa *et al.*, "Design and evaluation of a 3D transrectal ultrasound prostate biopsy system," Medical Physics, 35(10), 4695-4707 (2008).

[3] Fei, B., V. Master, P. Nieh *et al.*, "A PET/CT directed, 3D ultrasound-guided biopsy system for prostate cancer," Workshop on Prostate Cancer Imaging at the Medical Imaging Computing and Image Assisted Interventions Meeting (MICCAI 2011) - Lecture Notes in Computer Science. 6963, 100-108 (2011).

[4] Fei, B., W. S. Ng, S. Chauhan *et al.*, "The safety issues of medical robotics," Reliability Engineering & System Safety, 73(2), 183-192 (2001).

[5] Wei, Z., G. Wan, L. Gardi *et al.*, "Robot-assisted 3D-TRUS guided prostate brachytherapy: system integration and validation," Med.Phys., 31(3), 539-548 (2004).

[6] Schuster, D. M., J. R. Votaw, P. T. Nieh *et al.*, "Initial experience with the radiotracer anti-1-amino-3-18F-fluorocyclobutane-1-carboxylic acid with PET/CT in prostate carcinoma," J.Nucl.Med, 48(1), 56-63 (2007).

[7] Schuster, D., B. Fei, T. Fox *et al.*, "Histopathologic Correlation of Prostatic Adenocarcinoma on Radical Prostatectomy with Pre-Operative Anti-18F Fluorocyclobutyl-Carboxylic Acid Positron Emission Tomography/Computed Tomography," Laboratory Investigation, 91, 222A-223A (2011).

[8] Schilling, D., H. P. Schlemmer, P. H. Wagner *et al.*, "Histological verification of 11C-choline-positron emission/computed tomography-positive lymph nodes in patients with biochemical failure after treatment for localized prostate cancer," BJU.Int., 102(4), 446-451 (2008).

[9] Fei, B., H. Wang, C. Wu *et al.*, "Choline PET for monitoring early tumor response to photodynamic therapy," Journal of Nuclear Medicine, 51(1), 130 (2010).

[10] DeGrado, T. R., R. E. Coleman, S. Wang *et al.*, "Synthesis and evaluation of 18F-labeled choline as an oncologic tracer for positron emission tomography: initial findings in prostate cancer," Cancer Res., 61(1), 110-117 (2001).

[11] Oyama, N., H. Akino, H. Kanamaru *et al.*, "11C-acetate PET imaging of prostate cancer," J.Nucl.Med., 43(2), 181-186 (2002).

[12] Nunez, R., H. A. Macapinlac, H. W. Yeung *et al.*, "Combined 18F-FDG and 11C-methionine PET scans in patients with newly progressive metastatic prostate cancer," J.Nucl.Med., 43(1), 46-55 (2002).

[13] Akbari, H., X. Yang, L. Halig *et al.*, "3D Segmentation of Prostate Ultrasound Images using Wavelet Transform," Proceedings of SPIE, 7962, 79622K. (2011).

[14] Betrouni, N., M. Vermandel, D. Pasquier *et al.*, "Segmentation of abdominal ultrasound images of the prostate using a priori information and an adapted noise filter," Comput.Med.Imaging Graph., 29(1), 43-51 (2005).

[15] Chiu, B., G. H. Freeman, M. M. A. Salama *et al.*, "Prostate segmentation algorithm using dyadic wavelet transform and discrete dynamic contour," Physics in Medicine and Biology, 49(21), 4943-4960 (2004).

[16] Ding, M. Y., B. Chiu, I. Gyacskov *et al.*, "Fast prostate segmentation in 3D TRUS images based on continuity constraint using an autoregressive model," Medical Physics, 34(11), 4109-4125 (2007).

[17] Ghanei, A., H. Soltanian-Zadeh, A. Ratkewicz *et al.*, "A three-dimensional deformable model for segmentation of human prostate from ultrasound images," Med.Phys., 28(10), 2147-2153 (2001).

[18] Gong, L. X., S. D. Pathak, D. R. Haynor *et al.*, "Parametric shape modeling using deformable superellipses for prostate segmentation," Ieee Transactions on Medical Imaging, 23(3), 340-349 (2004).

[19] Kachouie, N. N., and P. Fieguth, "A medical texture local binary pattern for TRUS prostate segmentation.," Conf Proc IEEE Eng Med Biol Soc, 2007, 5605-5608 (2007).

[20] Liu, X., D. L. Langer, M. A. Haider *et al.*, "Prostate cancer segmentation with simultaneous estimation of Markov random field parameters and class.," IEEE Trans Med Imaging, 28(6), 906-915 (2009).

[21] Lixin, G., S. D. Pathak, D. R. Haynor *et al.*, "Parametric shape modeling using deformable superellipses for prostate segmentation," IEEE Transactions on Medical Imaging, 23, 340-349 (2004).

[22] Nanayakkara, N. D., J. Samarabandu, and A. Fenster, "Prostate segmentation by feature enhancement using domain knowledge and adaptive region based operations," Phys.Med.Biol., 51(7), 1831-1848 (2006).

[23] Pathak, S. D., D. R. Haynor, and Y. Kim, "Edge-guided boundary delineation in prostate ultrasound images," IEEE Transactions on Medical Imaging, 19(12), 1211-1219 (2000).

[24] Tutar, I. B., S. D. Pathak, L. X. Gong *et al.*, "Semiautomatic 3-D prostate segmentation from TRUS images using spherical harmonics," IEEE Transactions on Medical Imaging, 25(12), 1645-1654 (2006).

[25] Xu, R. S., O. Michailovich, and M. Salama, "Information tracking approach to segmentation of ultrasound imagery of the prostate.," IEEE Trans Ultrason Ferroelectr Freq Control, 57(8), 1748-1761 (2010).

[26] Yan, P., S. Xu, B. Turkbey *et al.*, "Adaptively Learning Local Shape Statistics for Prostate Segmentation in Ultrasound.," IEEE Trans Biomed Eng, 58, 633-641 (2010).

[27] Yang, F., J. Suri, and A. Fenster, "Segmentation of prostate from 3-D ultrasound volumes using shape and intensity priors in level set framework," Conf.Proc.IEEE Eng Med Biol.Soc.2006;, 1, 2341-2344 (2006).

[28] Yang, X. F., D. Schuster, V. Master *et al.*, "Automatic 3D Segmentation of Ultrasound Images Using Atlas Registration and Statistical Texture Prior," Proceedings of SPIE. 7964, 796432 (2011).
[29] Yu, Y., J. A. Molloy, and S. T. Acton, "Segmentation of the prostate from suprapubic ultrasound images," Med.Phys., 31(12), 3474-3484 (2004).
[30] Zhan, Y., and D. Shen, "Deformable segmentation of 3-D ultrasound prostate images using statistical texture matching method," IEEE Transactions on Medical Imaging, 25(3), 256-272 (2006).
[31] Zhang, Y., R. Sankar, and W. Qian, "Boundary delineation in transrectal ultrasound image for prostate cancer," Comput.Biol.Med., 37(11), 1591-1599 (2007).
[32] Badiei, S., S. E. Salcudean, J. Varah *et al.*, "Prostate segmentation in 2D ultrasound images using image warping and ellipse fitting," MICCAI, 4191, 17-24 (2006).
[33] Ladak, H. M., F. Mao, Y. Wang *et al.*, "Prostate boundary segmentation from 2D ultrasound images," Med.Phys., 27(8), 1777-1788 (2000).
[34] Zhang, H., Z. Bian, Y. Guo *et al.*, "An efficient multiscale approach to level set evolution," Engineering in Medicine and Biology Society.Proceedings of the 25th Annual International Conference of the IEEE, 1, 17-21 (2003).
[35] Zhan, Y. Q., and D. G. Shen, "Deformable segmentation of 3-D ultrasound prostate images using statistical texture matching method," IEEE Transactions on Medical Imaging, 25(3), 256-272 (2006).
[36] Shen, D., Y. Zhan, and C. Davatzikos, "Segmentation of prostate boundaries from ultrasound images using statistical shape model," IEEE Trans.Med.Imaging, 22(4), 539-551 (2003).
[37] Hodge, K. K., J. E. McNeal, M. K. Terris *et al.*, "Random systematic versus directed ultrasound guided transrectal core biopsies of the prostate," J.Urol., 142, 71-74 (1989).
[38] Fei, B. W., J. L. Duerk, D. B. Sodee *et al.*, "Semiautomatic nonrigid registration for the prostate and pelvic MR volumes," Academic Radiology, 12(7), 815-824 (2005).
[39] Fei, B., H. Wang, R. F. Muzic Jr *et al.*, "Deformable and rigid registration of MRI and microPET images for photodynamic therapy of cancer in mice," Medical Physics, 33, 753 (2006).
[40] Fei, B., S. Lee, D. Boll *et al.*, "Image Registration and Fusion for Interventional MRI Guided Thermal Ablation of the Prostate Cancer," Medical Image Computing And Computer-Assisted Intervention (MICCAI 2003) - Lecture Notes in Computer Science. 2879, 364-372 (2011).
[41] Fei, B., Z. Lee, D. T. Boll *et al.*, "Registration and fusion of SPECT, high-resolution MRI, and interventional MRI for thermal ablation of prostate cancer," Ieee Transactions on Nuclear Science, 51(1), 177-183 (2004).
[42] Fei, B., J. L. Duerk, and D. L. Wilson, "Automatic 3D registration for interventional MRI-guided treatment of prostate cancer.," Comput Aided Surg, 7(5), 257-267 (2002).
[43] Fei, B., J. L. Duerk, D. T. Boll *et al.*, "Slice-to-volume registration and its potential application to interventional MRI-guided radio-frequency thermal ablation of prostate cancer.," IEEE Trans Med Imaging, 22(4), 515-525 (2003).
[44] Fei, B., C. Kemper, and D. L. Wilson, "Three-dimensional warping registration of the pelvis and prostate," Proceedings of SPIE. 4684, 528-537 (2002).
[45] Fei, B., D. Boll, J. Duerk *et al.*, "Image Registration for Interventional MRI-Guided Minimally Invasive Treatment of Prostate Cancer," Proceedings of IEEE Engineering in Medicine and Biology (EMBS/BMES 2002) 2, 1185 (2002).
[46] Yang, X., H. Akbari, L. Halig *et al.*, "3D non-rigid registration using surface and local salient features for transrectal ultrasound image-guided prostate biopsy," Proceedings of SPIE. 7964, 79642V (2011).
[47] Manjunath, B. s., "Texture Features for Browsing and Retrieval of Image Data," IEEE Transactions on Pattern Analysis and Machine Intelligence, 18, 837-842 (1996).
[48] Vapnik, V. N., [The Nature of Statistical Learning Theory] Springer-Verlag, Berlin(1995).
[49] Wang, H., and B. Fei, "A modified fuzzy C-means classification method using a multiscale diffusion filtering scheme," Medical Image Analysis, 13(2), 193-202 (2009).
[50] Yang, X., and B. Fei, "A multiscale and multiblock fuzzy C-means classification method for brain MR images," Medical Physics, 38, 2879 (2011).
[51] Bogie, K., X. Wang, B. Fei *et al.*, "New technique for real-time interface pressure analysis: getting more out of large image data sets.," J Rehabil Res Dev, 45(4), 523-535 (2008).

Xiaofeng Yang and Baowei Fei, "3D prostate segmentation of ultrasound images combining longitudinal image registration and machine learning", Proc. SPIE 8316, 83162O (2012)

http://dx.doi.org/10.1117/12.912188